



INSTITUT DE FRANCE
Académie des sciences

Comptes Rendus

Physique

Yansheng Zhang, Gevorg Martirosyan, Christopher Junhong Ho, Jiří Etrych,
Christoph Eigen and Zoran Hadzibabic

Energy-space random walk in a driven disordered Bose gas


Volume 24, Special Issue S3 (2023), p. 153-171

Online since: 2 February 2024

Part of Special Issue: CNRS Gold Medal Jean Dalibard / *Médaille d'or du CNRS*
Jean Dalibard

Guest editors: Yvan Castin (Laboratoire Kastler Brossel (UMR 8552), Département de physique de l'ENS, Paris, France) and Klaus Mølmer (Institut Niels Bohr, Université de Copenhague, Danemark)

<https://doi.org/10.5802/crphys.168>

 This article is licensed under the
CREATIVE COMMONS ATTRIBUTION 4.0 INTERNATIONAL LICENSE.
<http://creativecommons.org/licenses/by/4.0/>



*The Comptes Rendus. Physique are a member of the
Mersenne Center for open scientific publishing*
www.centre-mersenne.org — e-ISSN : 1878-1535



CNRS Gold Medal Jean Dalibard / *Médaille d'or du CNRS*
Jean Dalibard

Energy-space random walk in a driven disordered Bose gas

Marche aléatoire dans l'espace des énergies d'un gaz de bosons forcé en présence de désordre

Yansheng Zhang^{*,a}, Gevorg Martirosyan^{*,a}, Christopher Junhong Ho^{*,a}, Jiří Etrych^{*,a}, Christoph Eigen^{*,*,a} and Zoran Hadzibabic^{*,a}

^a Cavendish Laboratory, University of Cambridge, J. J. Thomson Avenue, Cambridge CB3 0HE, UK

E-mails: yz661@cam.ac.uk (Y. Zhang), ce330@cam.ac.uk (C. Eigen)

We dedicate this work to Jean Dalibard, on the occasion of his CNRS Gold Medal

Abstract. Motivated by the experimental observation [1] that driving a non-interacting Bose gas in a 3D box with weak disorder leads to power-law energy growth, $E \propto t^\eta$ with $\eta = 0.46(2)$, and compressed-exponential momentum distributions that show dynamic scaling, we perform systematic numerical and analytical studies of this system. Schrödinger-equation simulations reveal a crossover from $\eta \approx 0.5$ to $\eta \approx 0.4$ with increasing disorder strength, hinting at the existence of two different dynamical regimes. We present a semi-classical model that captures the simulation results and allows an understanding of the dynamics in terms of an energy-space random walk, from which a crossover from $E \propto t^{1/2}$ to $E \propto t^{2/5}$ scaling is analytically obtained. The two limits correspond to the random walk being limited by the rate of the elastic disorder-induced scattering or the rate at which the drive can change the system's energy. Our results provide the theoretical foundation for further experiments.

Résumé. Motivés par l'observation expérimentale [1] que le forçage d'un gaz de bosons sans interaction dans une boîte 3D en présence d'un faible désordre conduit à une croissance de l'énergie en loi de puissance, $E \propto t^\eta$ avec $\eta = 0,46(2)$, et à des distributions en impulsion exponentielles comprimées révélant une loi d'échelle dynamique sous-jacente, nous effectuons des études numériques et analytiques systématiques de ce système. Des simulations de l'équation de Schrödinger montrent un passage de $\eta \approx 0,5$ à $\eta \approx 0,4$ lorsqu'on augmente la force du désordre, ce qui laisse supposer l'existence de deux régimes dynamiques différents. Nous présentons un modèle semi-classique qui rend compte des résultats des simulations et permet de comprendre la dynamique en termes de marche aléatoire dans l'espace des énergies, grâce à quoi un passage de la loi d'échelle $E \propto t^{1/2}$ à la loi $E \propto t^{2/5}$ est obtenu analytiquement. Les deux lois limites correspondent au fait que la marche aléatoire est limitée par le taux de la diffusion élastique induite par le désordre ou au contraire par le taux avec lequel le forçage peut modifier l'énergie du système. Nos résultats fournissent une base théorique aux futures études expérimentales.

Keywords. Ultracold atoms, Disordered system, Dynamic scaling, Continuous-time random walk, Chaos.

Mots-clés. Atomes froids, Système désordonné, Loi d'échelle dynamique, Marche aléatoire en temps continu, Chaos.

* Corresponding author.

Funding. The work was supported by EPSRC (Grant No. EP/P009565/1), ERC (UniFlat), and STFC (Grant No. ST/T006056/1). ZH acknowledges support from the Royal Society Wolfson Fellowship.

Manuscript received 7 July 2023, revised 29 September 2023 and 9 November 2023, accepted 14 November 2023.

1. Introduction

The emergence of simple and universal behaviours insensitive to system parameters and past trajectories is one of the most fascinating aspects of the physics of complex systems. Although the theory of universal behaviours was traditionally developed for equilibrium critical phenomena [2], recent experimental and theoretical studies have extended these ideas to a wide range of far-from-equilibrium systems [3–11].

In particular, a broad range of universal dynamics has been observed in quenched or driven ultracold atomic gases (see, e.g., [12–25]). One fruitful avenue for such studies involves driven box-trapped Bose gases [15], where the interplay of the drive and the inter-particle interactions leads to turbulent cascades with power-law momentum distributions [15] sustained by a constant momentum-space energy flux [26]. While interactions are usually central to the universal dynamics, in a recent experiment [1], we demonstrate that in absence of interactions, an interplay between drive and disorder can also lead to universal behaviour. This system, with a power-law energy growth ($E \propto t^\eta$ with $\eta = 0.46(2)$) and self-similar momentum distributions well characterised by a compressed exponential, shows qualitatively different behaviour from its interacting counterpart.

In Ref. [1], these observations are reproduced with Schrödinger-equation simulations and qualitatively explained by a semi-classical model. In this paper, we formalize our theoretical results. First, we extend the Schrödinger-equation simulations to a wider parameter range and observe a crossover from $\eta \approx 0.5$ to $\eta \approx 0.4$ with increasing disorder strength (Section 2), which hints at the existence of two distinct dynamical regimes. We then present the semi-classical model (Section 3) that captures the simulation results and allows an understanding of the dynamics in terms of an energy-space random walk. This in turn leads to a simple energy-space drift-diffusion equation (Section 4) that reproduces the crossover between the two regimes, and analytic predictions of $E \propto t^{1/2}$ and $E \propto t^{2/5}$ that emerge in the limits where the random walk is limited by the rate of disorder-induced scattering or the rate at which the drive can change the system's energy. Our results offer a new example of a dynamical system undergoing energy-space drift-diffusion [27–31] and provide the theoretical foundation for further experimental studies.

2. Schrödinger-equation simulations

The non-interacting dynamics in Ref. [1] can be described by the Schrödinger equation

$$i\hbar \frac{\partial}{\partial t} \psi = \left[-\frac{\hbar^2}{2m} \nabla^2 + V_{\text{box}} + V_{\text{D}} - \frac{Uz}{L} \sin(\omega t) \right] \psi, \quad (1)$$

where m is the particle mass, V_{box} is the clean trapping potential, V_{D} is the disorder, L is the box length along the driving-force direction \mathbf{z} , and U/L is the amplitude of the driving force. Here, we model the trap as a cubic box (Figure 1(a)) of infinite depth,¹ and the disorder V_{D} is chosen to be an uncorrelated (zero-mean) Gaussian random potential. The choice of an uncorrelated potential is sensible because the correlation length of V_{D} in an optical trap, which is on the order of the laser wavelength λ , is small compared to the atomic de-Broglie wavelength in the experiment. The strength of the random potential V_{D} is characterized by its r.m.s. value σ .

¹In Ref. [1], a cylindrical box trap was used, but the essential physics should be the same as long as the dynamics of the driven direction remain separable for $V_{\text{D}} = 0$.

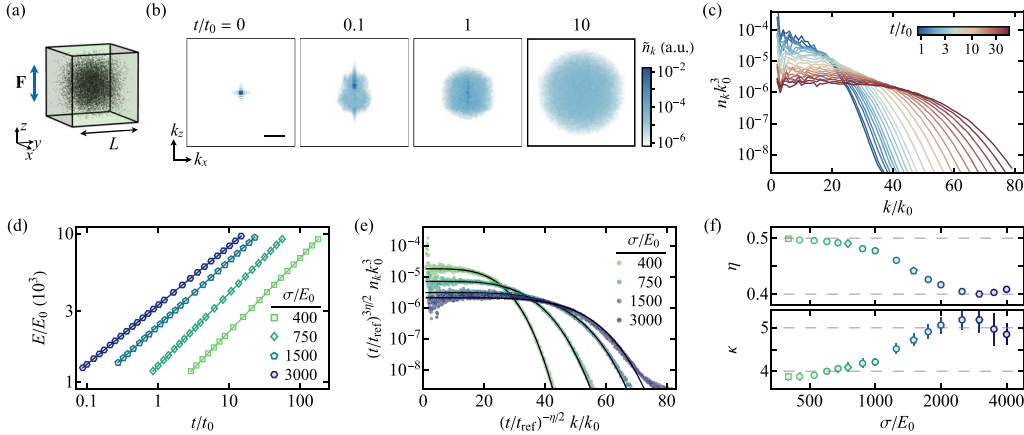


Figure 1. Schrödinger-equation simulations of a driven non-interacting Bose gas in a box with disorder. (a) Illustration of the simulation geometry. For the box of size L , the natural units of momentum, energy, and time are, respectively, $\hbar k_0 = \hbar\pi/L$, $E_0 = \hbar^2/(mL^2)$, and $t_0 = \hbar/E_0$. (b) Snapshots of the projected momentum distribution $\tilde{n}_k(k_x, k_z)$ for drive parameters $U = 1500 E_0$ and $\omega = 75 E_0/\hbar$, and disorder strength $\sigma = \langle V_D^2 \rangle^{1/2} = 750 E_0$ (the simulation grid is of size $127 \times 127 \times 127$, which leads to a UV cutoff of $127 k_0$). For comparison to Ref. [1], using the ^{39}K atom mass $m = 6.5 \times 10^{-26}$ kg and $L = 50 \mu\text{m}$, the simulation parameters here correspond to $U/k_B = 7.4$ nK, $\omega/(2\pi) = 9.5$ Hz, and $\sigma/k_B = 3.7$ nK. The scale bar corresponds to $20 k_0$. (c) Evolution of the (spherically averaged) momentum distribution n_k for parameters as in (b) and $t/t_0 \in [0.85, 55.8]$. (d) Energy-growth dynamics for $U = 1500 E_0$, $\omega = 75 E_0/\hbar$, and various σ . The solid lines show power-law fits used to extract the energy-time scaling exponent η . (e) For each σ value in (d), momentum distributions at different t (such as shown in (c) for $\sigma = 750 E_0$) collapse onto a single curve when dynamically scaled according to Equation (2), with arbitrarily chosen $t_{\text{ref}} = 10 t_0$. The solid lines show fits according to Equation (3), used to extract the compressed-exponential exponents κ . (f) Extracted η and κ as a function of σ for fixed $U = 1500 E_0$ and $\omega = 75 E_0/\hbar$.

In Figure 1(b), we illustrate the evolution of the momentum distribution, $n_k(\mathbf{k}) = |\psi(\mathbf{k})|^2$, for one choice of parameters $\{U, \omega, \sigma\}$. As in the experiment [1], the drive rapidly increases the momentum spread along \mathbf{z} , and cross-dimensional coupling due to V_D causes energy to leak into the transverse directions. At long times, $n_k(\mathbf{k})$ is nearly isotropic and gradually broadens (Figure 1(c)).

In agreement with the observations in Ref. [1], the energy growth is well described by a power-law, $E(t) \propto t^\eta$, as shown in Figure 1(d). The (nearly-)isotropic momentum distributions $n_k(k, t)$ at different t are self-similar, with

$$n_k(k, t) = \left(\frac{t}{t_{\text{ref}}}\right)^\alpha n_k\left(\left(\frac{t}{t_{\text{ref}}}\right)^\beta k, t_{\text{ref}}\right), \quad (2)$$

where t_{ref} is an arbitrary reference time, $\beta = -\eta/2$, and $\alpha = 3\beta$ corresponding to particle-conserving transport.² This self-similarity is illustrated in Figure 1(e) for different parameters $\{U, \omega, \sigma\}$; for each simulation, the distributions at different t collapse onto a single curve when rescaled according to Equation (2). The collapsed curves are well described by compressed exponentials (black lines in Figure 1(e)) of the form

$$n_k(k) \propto \exp[-(k/k_s)^\kappa], \quad (3)$$

with exponent κ and momentum scale $k_s \propto \sqrt{E}$.

In Ref. [1], only a relatively narrow range of η and κ was observed. Here, by extending the range of disorder strengths σ , we observe a crossover from $\eta \approx 0.5$ and $\kappa \approx 4$ to $\eta \approx 0.4$ and $\kappa \approx 5$ (Figure 1(f)). This hints at the existence of two distinct dynamical regimes, corresponding to weak and strong disorder. Analytically understanding the emergence of these two regimes is the goal of the subsequent sections.

3. Semi-classical model

The key ideas used to develop our model for the interplay of the drive and disorder are illustrated in Figure 2. First, we note that in the absence of disorder, strongly driving the gas along a separable axis of the trap leads to 1D chaotic dynamics with bounded energy growth [1, 32, 33]. This is illustrated by the (disorder-free) 1D Schrödinger-equation simulations shown in Figure 2(a), where we initialize the system in different sine-basis states $|\psi(t=0)\rangle = |k_{z,0}\rangle$ of the box (red dots). For small $k_{z,0}$, the strong drive mixes the k_z states only up to a cutoff k_c (horizontal dashed line), while for large $k_{z,0}$, the drive only weakly perturbs the system. However, the presence of disorder significantly modifies the picture in 3D. While the drive can only increase k_z up to about k_c , the disorder can scatter particles to equal-energy states with lower k_z , where the drive can again increase their energy (see Figure 2(b)). This cooperative process is the key to the unbounded energy growth.

To model this process, we propose the following semi-classical kinetic equation

$$\begin{aligned} \frac{\partial n_k(\mathbf{k}, t)}{\partial t} = & s|\mathbf{k}| \left[-n_k(\mathbf{k}, t) + \frac{2}{\pi|\mathbf{k}|^2} \int_{|\mathbf{k}|=|\mathbf{k}'|} n_k(\mathbf{k}', t) d^2\mathbf{k}' \right] \\ & + \Theta(k_c - k_z) f \left[-n_k(\mathbf{k}, t) + \frac{1}{k_c} \int_0^{k_c} n_k(k_x, k_y, k'_z, t) dk'_z \right], \end{aligned} \quad (4)$$

where $\Theta(k)$ is the Heaviside function, and s and f , respectively, characterize the rate of the elastic disorder-induced scattering and the rate at which the drive can change the system's energy.

The first line of Equation (4) describes the elastic disorder-induced scattering. A perturbative treatment using Fermi's golden rule gives the scattering rate from a state $|\mathbf{k}\rangle$ as

$$\Gamma_s(\mathbf{k}) = \frac{2\pi}{\hbar} \sum_{\mathbf{k}'} |\langle \mathbf{k} | V_D | \mathbf{k}' \rangle|^2 \delta[E(\mathbf{k}) - E(\mathbf{k}')]. \quad (5)$$

For uncorrelated V_D , after ensemble-averaging $|\langle \mathbf{k} | V_D | \mathbf{k}' \rangle|^2$ is \mathbf{k} -independent, so

$$\Gamma_s(\mathbf{k}) \simeq \langle \Gamma_s(\mathbf{k}) \rangle = s|\mathbf{k}|, \quad (6)$$

where $s \propto \sigma^2$ (see Appendix A.1), and the factor of k arises from the 3D density of states. This leads to the $-s|\mathbf{k}|n_k(\mathbf{k}, t)$ term in Equation (4) for the population *out-flux* from state $|\mathbf{k}\rangle$. The integral term in the first line of Equation (4) describes the *in-flux* to state $|\mathbf{k}\rangle$; since the out-flux from each state contributes an equal in-flux to every other state on the same k -shell, the total in-flux to state $|\mathbf{k}\rangle$ due to scattering is given by the out-flux averaged over the shell.

²In Ref. [1], line-of-sight integrated distributions were analysed experimentally, in which case $\alpha = 2\beta$, with β still equal to $-\eta/2$.

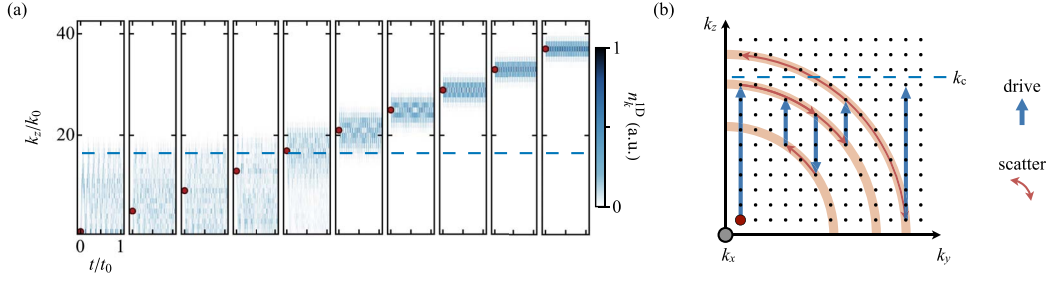


Figure 2. Key ideas underpinning our semi-classical model. (a) Numerical simulations of the (disorder-free) 1D Schrödinger equation for $U = 1500 E_0$ and $\omega = 75 E_0/\hbar$, starting from different initial sine-basis states (red dots). The density plots show the 1D momentum distribution $n_k^{\text{1D}}(k_z, t)$. The horizontal dashed line indicates the cutoff momentum k_c (see text and Appendix A.2). (b) The unbounded energy growth process in our model. The dots indicate the sine-basis eigenstates $|\mathbf{k}\rangle$ of the disorder-free box. At $t = 0$, the particles start in the ground state (red dot), and their k_z may be increased by the drive (blue arrows) up to k_c . The disorder-induced scattering (orange arrows) moves the particles along equal-energy shells and provides opportunities for the drive to further pump energy into the system.

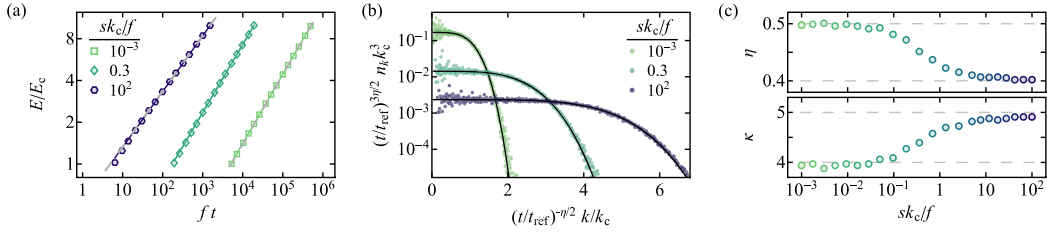


Figure 3. Stochastic-simulation results for our semi-classical model. (a) Energy growth over time for different sk_c/f . We normalize the energy E by $E_c = \hbar^2 k_c^2/(2m)$, and the time t by $1/f$. The colored lines are power-law fits used to extract η . The gray dashed lines show analytic predictions for $sk_c/f = 10^2$ and 10^{-3} using Equations (18) and (23), respectively. (b) Momentum distributions for the simulations shown in (a), dynamically scaled according to Equation (2), using the extracted η and an arbitrary reference time $t_{\text{ref}} = 5 \times 10^3/f$. The solid lines show compressed-exponential fits used to extract κ . (c) Extracted η and κ as a function sk_c/f , showing a similar crossover between the two dynamical regimes as seen in Figure 1(f).

The second line of Equation (4) heuristically models the driving process. While the chaotic 1D dynamics is not amenable to an exact treatment, the simulation results in Figure 2(a) inspire a simple model, where the drive randomly mixes k_z states up to k_c at a phenomenological rate f , without affecting states with $k_z > k_c$. While we also treat k_c phenomenologically, its value can be estimated from the time-averaged energy of the driven 1D system (see Appendix A.2).

Before analytically studying this model, we validate it through stochastic numerical simulations of Equation (4) for different values of the dimensionless parameter sk_c/f , which sets the ratio of the elastic scattering rate to the rate at which the drive can change the system's energy. As shown in Figure 3, our model, despite its simplicity, captures all the key features seen in the Schrödinger-simulation results in Figure 1.

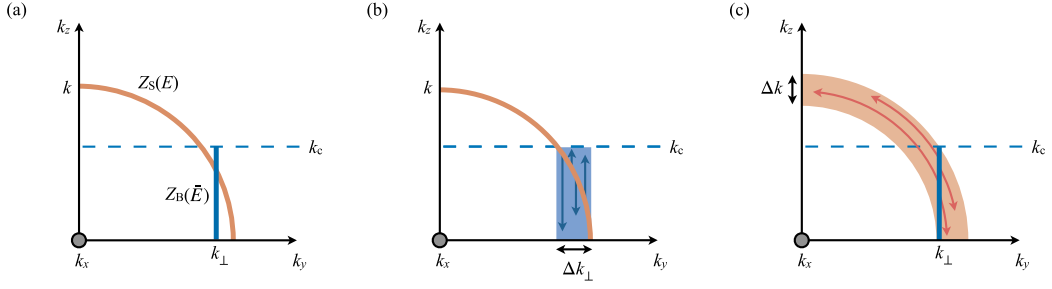


Figure 4. Qualitative ideas underpinning the energy-space random-walk picture. (a) Statistical states of the particle in energy space: $Z_S(E)$ (orange) labels the state of a particle randomly distributed on a spherical shell with definite k and E , while $Z_B(\bar{E})$ (blue) labels the state of a particle randomly distributed in a cylindrical band with definite k_\perp , random $k_z \in [0, k_c]$, and mean energy \bar{E} . (b) Effects of a driving event after scattering events. When the driving event happens, the particle originally in $Z_S(E)$ (orange line) may be driven into a range of $Z_B(\bar{E})$ states (blue shaded area) with a range (Δk_\perp) of k_\perp , and hence a range of \bar{E} . (c) Effects of a scattering event after driving events. When the scattering event happens, the particle originally in state $Z_B(\bar{E})$ (vertical blue line) may be scattered into $Z_S(E)$ states (orange shaded area) with a range (Δk) of k , and hence a range of E .

4. Analytic analysis

4.1. Qualitative ideas

To solve our model analytically, we switch from momentum space, where Equation (4) describes a highly non-local jump process, to energy space, where the process is quasi-local. In energy-space, the trajectory of a particle can be described by a sequence of events of the form

$$\begin{aligned} & \dots \xrightarrow{S} Z_S(E_1) \xrightarrow{S} Z_S(E_1) \xrightarrow{S} Z_S(E_1) \xrightarrow{D} Z_B(\bar{E}_2) \\ & \xrightarrow{D} Z_B(\bar{E}_2) \xrightarrow{S} Z_S(E_3) \xrightarrow{S} Z_S(E_3) \xrightarrow{D} Z_B(\bar{E}_4) \rightarrow \dots, \end{aligned}$$

where S and D refer to individual scattering and driving events, and $Z_S(E)$ and $Z_B(\bar{E})$ label the state of the particle, where the subscripts stand for *shell* and *band*, respectively (see Figure 4 (a)). After a scattering event S , the particle is randomly distributed on a k -shell of energy E , so its state is labeled $Z_S(E)$. Similarly, after a driving event D , the particle is randomly distributed on a cylindrical band with radius $k_\perp = (k_x^2 + k_y^2)^{1/2}$ and unknown $k_z \in [0, k_c]$, so only its mean energy $\bar{E} = \hbar^2(k_\perp^2 + k_c^2/3)/(2m)$ is known; we label such a state $Z_B(\bar{E})$. The fact that the particles can spend a significant time in $Z_B(\bar{E})$ means that the system is not necessarily in a micro-canonical ensemble, which is typically assumed in other related works [27–31].

Note that successive S or D events do not change the state Z_S or Z_B , but the state changes when S and D alternate, as illustrated in Figure 4(b) and (c). When the particle is in $Z_S(E)$, a D event can drive it into Z_B states with a range of possible k_\perp (see Δk_\perp in Figure 4(b)), and hence a range of \bar{E} distributed around the original energy E . Similarly, when the particle is in $Z_B(\bar{E})$, an S event can scatter it into Z_S states with a range of possible k (see Δk in Figure 4(c)), and hence a range of E distributed around the original energy \bar{E} . In both cases, the energy change can be of either sign and has an absolute value on the order of $E_c = \hbar^2 k_c^2/(2m)$. This suggests an energy-space random walk (with a reflecting boundary at $E = 0$, since E is constrained to be non-negative):

$$\frac{d}{dt} \langle E^2 \rangle \propto r(E) E_c^2, \quad (7)$$

where $r(E)$ is the (generally energy-dependent) rate at which S and D alternate. Due to the reflecting boundary, the mean energy $\langle E \rangle$ is non-zero and scales as $\langle E^2 \rangle^{1/2}$.

In the strong-scattering regime, $sk \gg f$, the rate $r(E)$ is limited by the occurrence of D events, so $r(E) \propto (k_c/k)f$, where the k_c/k factor arises because the particle takes part in the random walk only when $k_z < k_c$. Since $k = \sqrt{2mE}/\hbar \propto \langle E^2 \rangle^{1/4}$, Equation (7) implies

$$\langle E \rangle \propto E_c (ft)^{2/5}, \quad (8)$$

in agreement with both the Schrödinger-equation simulations and the stochastic simulations of our model.

On the other hand, in the strong-driving regime, $f \gg sk$, the rate $r(E)$ is limited by the occurrence of S events and given by $r(E) \propto (k_c/k)sk = sk_c$. As the suppression from k_c/k is cancelled by the density of states factor k in the scattering rate, Equation (7) implies

$$\langle E \rangle \propto E_c (sk_c t)^{1/2}, \quad (9)$$

which is also consistent with both the Schrödinger-equation simulations and the stochastic simulations of our model.

4.2. Energy-space drift-diffusion equation

We now formalize the ideas from Equation (7) and derive an energy-space drift-diffusion equation valid for all values of sk_c/f . Since the particle changes state only when S and D alternate, we can more succinctly describe its trajectory as

$$\dots \xrightarrow{\mathbf{S}} Z_S(E_1) \xrightarrow{\mathbf{D}} Z_B(\bar{E}_2) \xrightarrow{\mathbf{S}} Z_S(E_3) \xrightarrow{\mathbf{D}} \dots,$$

where \mathbf{S} and \mathbf{D} , respectively, stand for $D \dots DS$ and $S \dots SD$. Heuristically, the energy change may be described by

$$\frac{dE}{dt} = v_E + \zeta(t), \quad (10)$$

where the “velocity” v_E and “random force” $\zeta(t)$, respectively, lead to energy drift and diffusion. Denoting $\langle T_{S,D} \rangle$ as the mean waiting time for \mathbf{S} and \mathbf{D} to happen, and $\mu_{S,D}$ and $\sigma_{S,D}^2$ the energy drift and the energy-variance production in each step, we have

$$\begin{aligned} v_E &= \frac{\mu_S + \mu_D}{\langle T_S + T_D \rangle}, \\ \langle \zeta(t)\zeta(t') \rangle &= \frac{\sigma_S^2 + \sigma_D^2}{\langle T_S + T_D \rangle} \delta(t - t'). \end{aligned} \quad (11)$$

As derived in Appendix B, we have

$$\begin{aligned} \langle T_S + T_D \rangle &= \frac{k}{k_c} \left(\frac{1}{sk} + \frac{1}{f} \right), \\ \mu_S &= \frac{2fE_c^2}{45(sk + f)E}, \\ \mu_D &= 0, \\ \sigma_S^2 = \sigma_D^2 &= \frac{4E_c^2}{45}. \end{aligned} \quad (12)$$

The expressions for $\langle T_S + T_D \rangle$, μ_D , and $\sigma_{S,D}$ agree with the qualitative discussion in Section 4.1. The non-zero μ_S arises because a particle in $Z_B(\bar{E})$ is more likely to be scattered out of the band at higher k_z , due to the k dependence of the scattering rate.

Combining Equations (10)–(12), we can write a drift-diffusion equation [34] for the energy distribution $P(E, t)$:

$$\frac{\partial P}{\partial t} = \frac{4sfk_cE_c^2}{45} \frac{\partial}{\partial E} \left[\frac{1}{sk + f} \left(\frac{\partial P}{\partial E} - \frac{P}{2E} \right) \right]. \quad (13)$$

with s , f , k_c defined in Section 3, $E_c = \hbar^2 k_c^2 / (2m)$, and $k = \sqrt{2mE} / \hbar$. The formal derivation of Equation (13), using the theory of continuous-time random walks [35], is given in Appendix B. This equation satisfies the non-equilibrium fluctuation–dissipation relation proposed in Ref. [29], as discussed in Appendix C.

4.3. Limiting regimes

For $sk \gg f$, Equation (13) reduces to

$$\frac{\partial P}{\partial t} = D_d \frac{\partial}{\partial E} \left[\frac{1}{\sqrt{E}} \left(\frac{\partial P}{\partial E} - \frac{P}{2E} \right) \right], \quad (14)$$

with diffusion constant

$$D_d = \frac{4}{45} f E_c^{5/2}. \quad (15)$$

Following Ref. [36], Equation (14) can be shown to support self-similar solutions of the form

$$P(E, t) \propto \frac{E^{1/2}}{(D_d t)^{3/5}} \exp \left[-\frac{4E^{5/2}}{25D_d t} \right]. \quad (16)$$

The corresponding momentum distribution,

$$n_k(k, t) \propto \frac{1}{(D_d t)^{3/5}} \exp \left[-\frac{4\hbar^5 k^5}{25(2m)^{5/2} D_d t} \right], \quad (17)$$

is a compressed exponential (see Equation (3)) with $\kappa = 5$, and the energy growth is a power law

$$\langle E(t) \rangle = \left(\frac{5}{2} \right)^{4/5} \frac{1}{\Gamma(3/5)} (D_d t)^{2/5} = 1.398 (D_d t)^{2/5}, \quad (18)$$

with $\eta = 2/5$ in agreement with Equation (8).

For $sk \ll f$, Equation (13) reduces to

$$\frac{\partial P}{\partial t} = D_s \frac{\partial}{\partial E} \left[\frac{\partial P}{\partial E} - \frac{P}{2E} \right], \quad (19)$$

with diffusion constant

$$D_s = \frac{4}{45} s k_c E_c^2. \quad (20)$$

The self-similar solution supported by Equation (19) is

$$P(E, t) \propto \frac{E^{1/2}}{(D_s t)^{3/4}} \exp \left[-\frac{E^2}{4D_s t} \right]. \quad (21)$$

The corresponding momentum distribution,

$$n_k(k, t) \propto \frac{1}{(D_s t)^{3/4}} \exp \left[-\frac{\hbar^4 k^4}{16m^2 D_s t} \right], \quad (22)$$

is a compressed exponential with $\kappa = 4$, and the energy growth is a power law

$$\langle E(t) \rangle = \frac{\Gamma(1/4)}{2\Gamma(3/4)} (D_s t)^{1/2} = 1.479 (D_s t)^{1/2}, \quad (23)$$

with $\eta = 1/2$ in agreement with Equation (9).

To quantitatively verify Equations (18) and (23), in Figure 3(a), we compare them to our stochastic-simulation results for $sk_c/f = 10^2$ and 10^{-3} and observe good agreement.

In the low-disorder limit ($sk \ll f$), we can also directly compare our analytically predicted energy-diffusion coefficient D_s (Equation (20)) with the Schrödinger-equation simulations, because D_s depends only on s and k_c , both of which can be obtained from the input parameters $\{U, \omega, \sigma\}$ (such a comparison is not possible for D_d because we cannot calculate f). For each

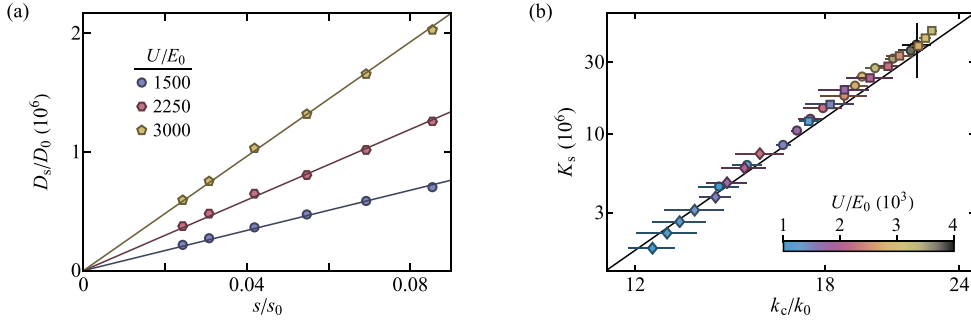


Figure 5. Comparison between analytic predictions and Schrödinger-equation simulations in the low-disorder regime ($sk \ll f$). (a) Energy-space diffusion coefficient D_s (in units of $D_0 = E_0^3/\hbar$) extracted from simulations with $\omega = 75 E_0/\hbar$, plotted versus s (in units of $s_0 = E_0 L/\hbar$) analytically calculated from σ . The solid lines show the linear fits to $D_s/D_0 = K_s s/s_0$, used to extract the proportionality constant K_s . (b) K_s versus calculated k_c (see Appendix A.2) for different U (color bar) and ω (diamonds: $50 E_0/\hbar$, circles: $75 E_0/\hbar$, and squares: $100 E_0/\hbar$). The solid line shows the analytic prediction $K_s = (\pi k_c/k_0)^5/45$ (calculated from Equation (20)) with no free parameters.

simulation in the low-disorder limit,³ we fit the $E(t)$ curve (such as shown in Figure 1(d)) to Equation (23) and extract D_s . In Figure 5(a), for fixed ω and various U , we plot the extracted D_s versus s calculated from σ and observe the linear behaviour predicted in Equation (20). Then, in Figure 5(b), for several ω and a range of U , we show that the fitted constants of proportionality between D_s and s (the slopes of lines in Figure 5(a)) agree with Equation (20).

4.4. General solution

After analysing the two limits, we now examine the general solution to Equation (13). We can remove the parameters $\{s, k_c, f\}$ from the equation by introducing the dimensionless quantities

$$k' = \frac{k}{k_{\text{sys}}}, \quad E' = \frac{E}{E_{\text{sys}}}, \quad t' = \frac{t}{t_{\text{sys}}}, \quad (24)$$

with

$$k_{\text{sys}} = \frac{f}{s}, \quad E_{\text{sys}} = \frac{\hbar^2 k_{\text{sys}}^2}{2m}, \quad t_{\text{sys}} = \frac{f^4}{s^5 k_c^5}. \quad (25)$$

This transforms Equation (13) to

$$\frac{\partial P'}{\partial t'} = \frac{4}{45} \frac{\partial}{\partial E'} \left[\frac{1}{k' + 1} \left(\frac{\partial P'}{\partial E'} - \frac{P'}{2E'} \right) \right], \quad (26)$$

with $P'(E', t') = E_{\text{sys}} P(E, t)$.

This shows that, under appropriate scaling, solutions to Equation (13) follow a universal E - t trajectory. We illustrate this in Figure 6. In principle, at very long times, one should always observe $E \propto t^{2/5}$ and $\kappa = 5$. In terms of system parameters, we classify the system as low-disorder if $sk_c \ll f$ and high-disorder if $sk_c \gg f$, but the dynamics is actually controlled by the ratio sk/f , which increases as the energy grows. Thus, a low-disorder system at long times is mathematically identical to a high-disorder one at short times. However, note that the crossover between the two regimes occurs over an enormous timescale, so any realistic experiment will sample a small region of the universal trajectory, with the energy growth well fitted by a power

³We define the low-disorder limit here to correspond to $\eta > 0.48$ (as obtained from an unconstrained fit).

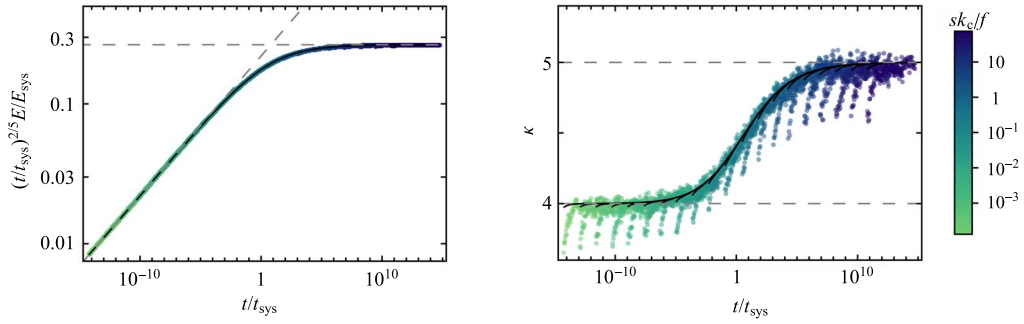


Figure 6. Results of extended stochastic simulations of the semi-classical model with different sk_c/f . We show the evolution of the energy E (left) and of the compressed-exponential exponent κ for the instantaneous shape of n_k (right). We perform simulations with different sk_c/f , indicated by the color, which merge into common curves when t and E are scaled using units given in Equation (25). In both plots, the dashed lines show the analytic predictions in the two limiting regimes, and the solid black lines show numerical predictions using Equation (13). The small deviations of stochastic simulations from the solid lines (not visible in the E plot) arise due to initial transients in each simulation.

law and an essentially constant κ . Also note that for a strongly disordered system, t_{sys} is very short ($sk_c/f \gg 1$, so $t_{\text{sys}} \ll 1/f$), so by the time any significant energy is pumped into the system, t/t_{sys} is already large.

5. Conclusion and outlook

In conclusion, we have developed a semi-classical model for a driven non-interacting box-trapped Bose gas in the presence of uncorrelated disorder. The dynamics at the heart of this model can be understood in terms of an energy-space random walk, and the resulting analytic predictions reproduce the key features seen both in the experiment of Ref. [1] and in Schrödinger-equation simulations.

Our work points to several future directions. First, it would be interesting to experimentally explore the dynamics beyond the weak-disorder regime. This could also lead to further theoretical questions, as the scattering in our model is treated within first-order perturbation theory, which does not hold for arbitrarily strong disorder; for example, the onset of Anderson localization [37] may lead to additional dynamical regimes. Second, an analogous study in 2D may reveal even richer physics. Taking our model at face value, we would expect $\eta = 2/5$ across all parameter regimes in 2D, because there is no density-of-states enhancement factor k in the scattering rate, so we always have $r \propto 1/k$ and $E \propto t^{2/5}$. However, this may be inaccurate due to the more prominent role of fluctuations in 2D. For example, our treatment of the scattering rate relies on ensemble-averaging. While this is a good approximation in 3D, its validity in 2D is not obvious, as far fewer states are involved in the scattering process. This poses interesting questions both experimentally and theoretically.

Data availability

The data and code that support the findings of this study are available in the Apollo repository (<https://doi.org/10.17863/CAM.105357>).

Declaration of interests

The authors do not work for, advise, own shares in, or receive funds from any organization that could benefit from this article, and have declared no affiliations other than their research organizations.

Appendix A. Calculation of the semi-classical model parameters

A.1. The scattering rate

In this section, we present the calculation for $\Gamma_s(\mathbf{k})$ in Equation (5) and derive an explicit expression for s in Equation (6) for a cubic box of volume L^3 in the presence of a disorder potential $V_D(\mathbf{r})$. The unperturbed basis states of the box are $|\mathbf{k}\rangle$ states of the form

$$|\mathbf{k}\rangle = \sqrt{\frac{8}{L^3}} \Sigma(\mathbf{k}, \mathbf{r}) = \sqrt{\frac{8}{L^3}} \sin(k_x x) \sin(k_y y) \sin(k_z z). \quad (\text{A27})$$

The ensemble-averaged matrix element $\langle\langle |\langle \mathbf{k} | V_D(\mathbf{r}) | \mathbf{k}' \rangle|^2 \rangle\rangle$ is explicitly

$$\begin{aligned} \langle\langle |\langle \mathbf{k} | V_D(\mathbf{r}) | \mathbf{k}' \rangle|^2 \rangle\rangle &= \left\langle\left\langle \left| \frac{8}{L^3} \int \Sigma(\mathbf{k}, \mathbf{r}) V_D(\mathbf{r}) \Sigma(\mathbf{k}', \mathbf{r}) d^3 \mathbf{r} \right|^2 \right\rangle\right\rangle \\ &= \frac{64}{L^6} \int \Sigma(\mathbf{k}, \mathbf{r}_1) \Sigma(\mathbf{k}', \mathbf{r}_1) \Sigma(\mathbf{k}, \mathbf{r}_2) \Sigma(\mathbf{k}', \mathbf{r}_2) \langle\langle V_D(\mathbf{r}_1) V_D(\mathbf{r}_2) \rangle\rangle d^3 \mathbf{r}_1 d^3 \mathbf{r}_2 \\ &= \frac{64}{L^6} \int \Sigma(\mathbf{k}, \mathbf{r}_1) \Sigma(\mathbf{k}', \mathbf{r}_1) \Sigma(\mathbf{k}, \mathbf{r}_2) \Sigma(\mathbf{k}', \mathbf{r}_2) C(\mathbf{r}_1 - \mathbf{r}_2) d^3 \mathbf{r}_1 d^3 \mathbf{r}_2, \end{aligned} \quad (\text{A28})$$

where

$$C(\mathbf{r}_1 - \mathbf{r}_2) = \langle\langle V_D(\mathbf{r}_1) V_D(\mathbf{r}_2) \rangle\rangle. \quad (\text{A29})$$

By substituting the Fourier representation

$$C(\mathbf{r}_1 - \mathbf{r}_2) = \frac{1}{(2\pi)^3} \int \tilde{C}(\mathbf{q}) e^{i\mathbf{q} \cdot (\mathbf{r}_1 - \mathbf{r}_2)} d^3 \mathbf{q} \quad (\text{A30})$$

into Equation (A28), we get

$$\begin{aligned} \langle\langle |\langle \mathbf{k} | V_D(\mathbf{r}) | \mathbf{k}' \rangle|^2 \rangle\rangle &= \frac{64}{(2\pi)^3 L^6} \int \Sigma(\mathbf{k}, \mathbf{r}_1) \Sigma(\mathbf{k}', \mathbf{r}_1) \Sigma(\mathbf{k}, \mathbf{r}_2) \Sigma(\mathbf{k}', \mathbf{r}_2) \tilde{C}(\mathbf{q}) e^{i\mathbf{q} \cdot (\mathbf{r}_1 - \mathbf{r}_2)} d^3 \mathbf{r}_1 d^3 \mathbf{r}_2 d^3 \mathbf{q} \\ &= \frac{64}{(2\pi)^3 L^6} \int \left| \int \Sigma(\mathbf{k}, \mathbf{r}) \Sigma(\mathbf{k}', \mathbf{r}) e^{i\mathbf{q} \cdot \mathbf{r}} d^3 \mathbf{r} \right|^2 \tilde{C}(\mathbf{q}) d^3 \mathbf{q}. \end{aligned} \quad (\text{A31})$$

The $\{x, y, z\}$ integrals are separable, with 1D integrals of the form

$$\begin{aligned} I_{1D} &= \left| \int_0^L \sin(kx) \sin(k'x) e^{iqx} dx \right|^2 \\ &= \frac{L^2}{16} \left| \text{sinc}\left(\frac{(k+k'+q)L}{2}\right) e^{i(k+k'+q)L/2} + \text{sinc}\left(\frac{(k+k'-q)L}{2}\right) e^{i(k+k'-q)L/2} \right. \\ &\quad \left. - \text{sinc}\left(\frac{(k-k'+q)L}{2}\right) e^{i(k-k'+q)L/2} - \text{sinc}\left(\frac{(k-k'-q)L}{2}\right) e^{i(k-k'-q)L/2} \right|^2. \end{aligned} \quad (\text{A32})$$

For large momenta, the sinc functions in the above equation have almost no overlap, so we can drop the interference terms:

$$\begin{aligned} I_{1D} &\simeq \frac{L^2}{16} \left\{ \text{sinc}^2\left(\frac{(k+k'+q)L}{2}\right) + \text{sinc}^2\left(\frac{(k+k'-q)L}{2}\right) \right. \\ &\quad \left. + \text{sinc}^2\left(\frac{(k-k'+q)L}{2}\right) + \text{sinc}^2\left(\frac{(k-k'-q)L}{2}\right) \right\}, \end{aligned} \quad (\text{A33})$$

and using $\lim_{L \rightarrow \infty} \text{sinc}^2(qL/2) = (2\pi/L) \delta(q)$, we get

$$I_{1D} \simeq \frac{L\pi}{8} [\delta(k+k'+q) + \delta(k+k'-q) + \delta(k-k'+q) + \delta(k-k'-q)]. \quad (\text{A34})$$

Substituting this expression back into Equation (A31), we get

$$\langle\langle |\langle \mathbf{k} | V_D(\mathbf{r}) | \mathbf{k}' \rangle|^2 \rangle\rangle = \frac{1}{64L^3} \sum_{\mathbf{k}''} \tilde{C}(\mathbf{k}''), \quad (\text{A35})$$

with $\mathbf{k}'' = (\lambda_x k_x + \lambda'_x k'_x, \lambda_y k_y + \lambda'_y k'_y, \lambda_z k_z + \lambda'_z k'_z)$ where λ_i, λ'_i can take on values ± 1 . Intuitively, $\{\mathbf{k}''\}$ is the set of 64 \mathbf{k} -vectors that connect the plane-wave components in $|\mathbf{k}\rangle$ to those in $|\mathbf{k}'\rangle$.

In numerical simulations, we discretize real space into $(N-1)^3$ grid points, which requires some changes to the above equations. First, the decomposition of the $C(\mathbf{r}_1 - \mathbf{r}_2)$ is written in terms of a Fourier series rather than a Fourier transform,

$$C(\mathbf{r}_1 - \mathbf{r}_2) = \frac{1}{L^3} \sum_{\mathbf{q}} \tilde{C}(\mathbf{q}) e^{i\mathbf{q} \cdot (\mathbf{r}_1 - \mathbf{r}_2)}, \quad (\text{A36})$$

where the summation is performed over the first Brillouin zone of the grid. Second, the delta functions $\delta(\mathbf{k}'' - \mathbf{q})$ become $\sum_{\mathbf{G}} \delta_{\mathbf{k}'' - \mathbf{q}, \mathbf{G}}$ where $\{\mathbf{G}\}$ is the set of reciprocal lattice vectors. This change introduces unphysical Umklapp scattering processes. However, for the uncorrelated disorder potential $V_D(\mathbf{r})$ with zero mean and variance σ^2 , the correlation function is $C(\mathbf{r}) = \delta_{\mathbf{r},0} \sigma^2$, so $\tilde{C}(\mathbf{k}'')$ is constant and the Umklapp scattering processes do not affect the physics. Equation (A35) then gives

$$\langle\langle |\langle \mathbf{k} | V_D(\mathbf{r}) | \mathbf{k}' \rangle|^2 \rangle\rangle = \frac{\sigma^2}{N^3}. \quad (\text{A37})$$

Note that the factor of $1/64$ in Equation (A35) disappears because all 64 \mathbf{k}'' contribute to the sum. Finally, substituting Equation (A37) into Equation (5), we get

$$\Gamma_s(\mathbf{k}) = \frac{2\pi}{\hbar} \sum_{\mathbf{k}'} |\langle \mathbf{k} | V_D(\mathbf{r}) | \mathbf{k}' \rangle|^2 \delta[E(\mathbf{k}) - E(\mathbf{k}')] = \frac{mL^3}{\pi N^3 \hbar^3} \sigma^2 k, \quad (\text{A38})$$

where the sum has been approximated by an integral and we can read off the scattering parameter s in Equation (6) as

$$s = \frac{mL^3}{\pi N^3 \hbar^3} \sigma^2. \quad (\text{A39})$$

A.2. The cutoff momentum k_c

Here we detail our method to determine k_c . In our semi-classical model, we have assumed that the drive randomly mixes states with $k_z < k_c$ at a rate f . Therefore, in 1D, a state initialized with $k_{z,0} < k_c$ will reach a momentum distribution n_k^{1D} that is (on average) uniform below k_c and zero above it. For $k_{z,0} < k_c$, the mean energy of the driven system is thus

$$\langle E \rangle = \frac{1}{k_c} \int_0^{k_c} \frac{\hbar^2}{2m} k_z^2 dk_z = \frac{\hbar^2}{6m} k_c^2 = \frac{1}{3} E_c. \quad (\text{A40})$$

Therefore, k_c may be estimated by computing $\langle E \rangle$ from 1D Schrödinger-equation simulations for a driven particle in a disorder-free box. In Figure 7(a), we show $\langle E \rangle$ for $U = 1500 E_0$ and $\omega = 75 E_0 / \hbar$, starting from different $k_{z,0}$. For low $k_{z,0}$, $\langle E \rangle$ is indeed essentially independent of $k_{z,0}$ (see also Figure 2(a)). To estimate k_c and its error, we use the mean and the standard deviation of $\langle E \rangle$ for $k_{z,0} < 10 k_0$. Figure 7(b) shows the values of k_c calculated for the values of U and ω used in Figure 5(b).

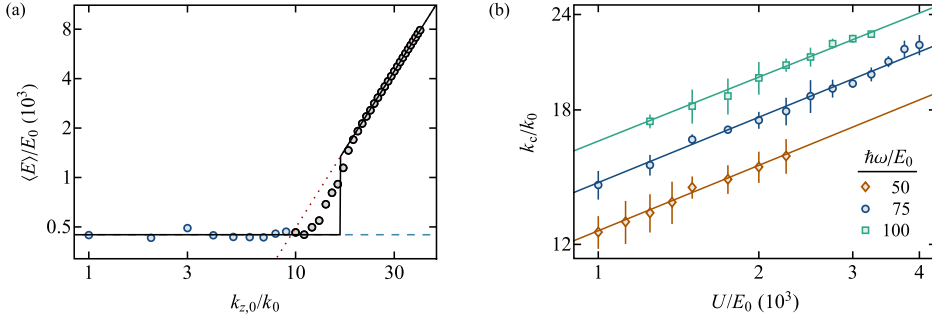


Figure 7. Extraction of k_c from 1D Schrödinger-equation simulations without disorder. (a) Time-averaged energy, $\langle E \rangle$, for the system initialized in different states $k_{z,0}$; see also Figure 2(a). We normalise $k_{z,0}$ by $k_0 = \pi/L$ and $\langle E \rangle$ by $E_0 = \hbar^2/(mL^2)$. The solid line shows the prediction of our model: For $k_{z,0} < k_c$, the particles evenly probe momentum states up to k_c , so $\langle E \rangle = E_c/3$ independently of $k_{z,0}$ (blue dashed line), while for $k_{z,0} > k_c$, we have $\langle E \rangle = \hbar^2 k_{z,0}^2/(2m)$ (red dotted line), so at $k_{z,0} = k_c$ the energy jumps by a factor of 3. (b) Extracted values of k_c for all the simulation parameters used in Figure 5(b). The solid lines are guides to the eye.

Appendix B. Derivation of the energy drift-diffusion equation

As described in Section 4.2, the trajectory of a particle whose distribution is described by Equation (4) can be summarized as

$$\dots \xrightarrow{\mathbf{S}} Z_S(E_1) \xrightarrow{\mathbf{D}} Z_B(\bar{E}_2) \xrightarrow{\mathbf{S}} Z_S(E_3) \xrightarrow{\mathbf{D}} Z_B(\bar{E}_4) \xrightarrow{\mathbf{S}} Z_S(E_5) \xrightarrow{\mathbf{D}} \dots, \quad (\text{B41})$$

where \mathbf{S} and \mathbf{D} refer to $D \dots DS$ and $S \dots SD$, respectively. In this section, we first calculate the distributions of the waiting times $T_{S,D}$, the energy drifts $\mu_{S,D}(E)$, and the energy variances $\sigma_{S,D}^2(E)$, before assembling the drift-diffusion equation (Equation (13)). Note that in this section we set $\hbar = m = L = 1$.

B.1. Calculations for $\mathbf{D} = S \dots SD$

B.1.1. Calculation of T_D

The waiting time T_D is a continuous random variable. We begin by calculating its mean, $\langle T_D \rangle$, before calculating its full distribution. Suppose that at $t = 0$, the particle has just been scattered into $Z_S(E)$ with unknown position on the k -shell. Then, with probability $(1 - k_c/k)$, it sits in the upper part of the shell (“upper shell”), where $k_z > k_c$. In this case, the next event has to be S , and the waiting time for it is $\text{Exp}[sk]$ (an exponential distribution with time constant $1/(sk)$). After the S event, the clock is reset because the particle is still in the same statistical state Z_S . Therefore, the additional waiting time before D happens is again T_D . Hence,

$$T_{D|u} = \text{Exp}[sk] + T_D, \quad (\text{B42})$$

where $T_{D|u}$ is the conditional waiting time till D if the particle is initially in the upper shell. On the other hand, if the particle is initially in the lower shell, where $k_z < k_c$, the next event could be either S or D , and the waiting time for this event is $\text{Exp}[sk + f]$. With probability $f/(sk + f)$, the

event is D , and the particle is driven out of the shell. Otherwise, the event is S , the clock is reset, and the additional waiting time before D happens is again T_D . This can be written as

$$\begin{aligned} T_{D|\ell,D} &= \text{Exp}[sk + f], \\ T_{D|\ell,S} &= \text{Exp}[sk + f] + T_D, \end{aligned} \quad (\text{B43})$$

where $T_{D|\ell,S}$ and $T_{D|\ell,D}$ are the conditional waiting times till D if the particle is initially in the lower shell and the first event after $t = 0$ is S or D , respectively. We can thus write an equation for $\langle T_D \rangle$:

$$\langle T_D \rangle = \frac{k - k_c}{k} \left(\frac{1}{sk} + \langle T_D \rangle \right) + \frac{k_c}{k} \left\{ \frac{f}{sk + f} \frac{1}{sk + f} + \frac{sk}{sk + f} \left(\frac{1}{sk + f} + \langle T_D \rangle \right) \right\}. \quad (\text{B44})$$

The solution for $\langle T_D \rangle$ is

$$\langle T_D \rangle = \frac{k}{k_c} \frac{1}{f} + \frac{k - k_c}{k_c} \frac{1}{sk}. \quad (\text{B45})$$

For $k \gg k_c$, to leading order in k_c ,

$$\langle T_D \rangle \simeq \frac{k}{k_c} \frac{1}{f} + \frac{1}{sk_c}. \quad (\text{B46})$$

Generalizing the analysis above, we can also write an equation for the distribution function $\phi_D(t)$ for T_D :

$$\begin{aligned} \phi_D(t) &= \frac{k - k_c}{k} \int_0^t g(t - t'; sk) \phi_D(t') dt' \\ &\quad + \frac{k_c}{k} \left(\frac{f}{sk + f} g(t; sk + f) + \frac{sk}{sk + f} \int_0^t g(t - t'; sk + f) \phi_D(t') dt' \right), \end{aligned} \quad (\text{B47})$$

where $g(t; \lambda)$ denotes the exponential distribution function with time constant $1/\lambda$. By taking the Laplace transform

$$\tilde{\phi}_D(u) = \mathcal{L}[\phi_D] = \int_0^\infty \phi_D(t) e^{-ut} dt, \quad (\text{B48})$$

the integral equation (B47) can be reduced to an algebraic one,

$$\tilde{\phi}_D(u) = \frac{k - k_c}{k} \frac{sk}{u + sk} \tilde{\phi}_D(u) + \frac{k_c}{k} \left(\frac{f}{sk + f} \frac{sk + f}{u + sk + f} + \frac{sk}{sk + f} \frac{sk + f}{u + sk + f} \tilde{\phi}_D(u) \right). \quad (\text{B49})$$

Its solution is

$$\tilde{\phi}_D(u) = \frac{k_c}{k} \frac{f u + s f k}{u^2 + (sk + f)u + f s k_c}. \quad (\text{B50})$$

The exact expression for $\phi_D(t)$, obtained from the inverse Laplace transform of $\tilde{\phi}_D(u)$, is complicated, but it can be well approximated by an exponential distribution. This can be seen from the above equation, where for small u (corresponding to large t and large k), we have (using $\langle T_D \rangle$ in Equation (B46))

$$\tilde{\phi}_D(u) \simeq \frac{k_c}{k} \frac{s f k}{(sk + f)u + f s k_c} \simeq \frac{1/\langle T_D \rangle}{u + 1/\langle T_D \rangle} = \mathcal{L} \left[\frac{1}{\langle T_D \rangle} e^{-t/\langle T_D \rangle} \right]. \quad (\text{B51})$$

B.1.2. Calculation of $\mu_D(E)$ and $\sigma_D^2(E)$

When $Z_S(E) \xrightarrow{D} Z_B(\bar{E})$ happens, the new energy \bar{E} is a random variable with distribution $G(\bar{E}|E)$. Irrespective of T_D , it is equally likely for the particle to be driven from any point on the lower shell. This means that

$$G(\bar{E}|E) d\bar{E} \propto 2\pi k^2 \sin\theta d\theta \propto \frac{k k_\perp}{\sqrt{k^2 - k_\perp^2}} dk_\perp, \quad (\text{B52})$$

with $k_{\perp} \in [\sqrt{k^2 - k_c^2}, k]$ because the particle is in the lower shell. After some manipulation, we get

$$G(\bar{E}|E) \propto \frac{1}{\sqrt{E - \bar{E} + k_c^2/6}}, \quad (\text{B53})$$

with $\bar{E} - E \in [-k_c^2/3, k_c^2/6]$. From this distribution, we calculate

$$\begin{aligned} \mu_D(E) &= \langle \bar{E} - E \rangle = 0, \\ \sigma_D^2(E) &= \langle (\bar{E} - E)^2 \rangle = \frac{1}{45} k_c^4. \end{aligned} \quad (\text{B54})$$

B.2. Calculations for $\mathbf{S} = D \dots DS$

B.2.1. Calculation of T_S

The waiting time T_S is calculated along the same lines as T_D above, but we need to also average over the initial k_z in the band (with fixed k_{\perp}) since the scattering rate sk depends on k_z via $k = \sqrt{k_{\perp}^2 + k_z^2}$. This gives

$$\langle T_S \rangle = \frac{1}{k_c} \int_0^{k_c} \left[\frac{1}{sk + f} + \frac{f}{sk + f} \langle T_S \rangle \right] dk_z, \quad (\text{B55})$$

where the first term in the integral comes from the mean waiting time till the first event (either D or S) after $t = 0$, and the second term comes from the additional time needed if the first event is D . Solving the equation, we get

$$\langle T_S \rangle = \left[\int_0^{k_c} \frac{sk}{sk + f} dk_z \right]^{-1} \int_0^{k_c} \frac{1}{sk + f} dk_z \simeq \frac{1}{\sqrt{2\bar{E}_S}} + O(k_c^4). \quad (\text{B56})$$

Note that the integrals in the above equation cannot be evaluated analytically, but by treating k_c and k_z as small parameters, we can perform Taylor expansions and obtain the simple result above.

It is also possible to obtain the distribution of T_S using the Laplace transform,

$$\tilde{\phi}_S(u) = \left[\int_0^{k_c} \frac{u + sk}{u + sk + f} dk_z \right]^{-1} \int_0^{k_c} \frac{sk}{u + sk + f} dk_z \simeq \frac{1/\langle T_S \rangle}{u + 1/\langle T_S \rangle} + O(k_c^4). \quad (\text{B57})$$

Therefore, the distribution for T_S is also exponential to leading order.

B.2.2. Calculation of $\mu_S(\bar{E})$ and $\sigma_S^2(\bar{E})$

When $Z_B(\bar{E}) \xrightarrow{S} Z_S(E)$ happens, the new energy E is a random variable. The exact distribution for E is tricky to calculate because it is correlated with T_S . In particular, if the particle is scattered when it has a higher k_z (and hence a higher k), E will be larger, and T_S is likely to have been shorter due to the k -dependence of the scattering rate. However, for an approximate calculation, we ignore this correlation and calculate the distribution of E irrespective of T_S . The error of this approximation is a higher-order term.

First, let us calculate the probability $p(k_z|\bar{E})$ that the particle is scattered out at k_z , and hence into the shell with $E = (k_{\perp}^2 + k_z^2)/2$. If the particle is at k'_z at $t = 0$, then, with probability $sk'/(sk' + f)$, the first event after $t = 0$ is S , and we get a contribution to $p(k_z|\bar{E})$ only if $k'_z = k_z$; otherwise, with probability $f/(sk' + f)$, the first event after $t = 0$ is D , and the probability that the particle leaves at k_z in some future S event is $p(k_z|\bar{E})$. Averaging over k'_z , we get

$$p(k_z|\bar{E}) = \frac{1}{k_c} \int_0^{k_c} \left[\frac{sk'}{sk' + f} \delta(k_z - k'_z) + \frac{f}{sk' + f} p(k_z|\bar{E}) \right] dk'_z, \quad (\text{B58})$$

where $k = \sqrt{k_\perp^2 + k_z^2}$ and $k' = \sqrt{k_\perp'^2 + k_z'^2}$. Solving the equation, we get

$$p(k_z|\bar{E}) = \left[\int_0^{k_c} \frac{sk'}{sk' + f} dk_z' \right]^{-1} \frac{sk}{sk + f}. \quad (\text{B59})$$

Since $E = k^2/2$, we can calculate

$$\begin{aligned} \mu_S(\bar{E}) &= \langle E - \bar{E} \rangle = \frac{fk_c^4}{90\bar{E}(f + \sqrt{2\bar{E}s})} + O(k_c^6), \\ \sigma_S^2(\bar{E}) &= \langle (E - \bar{E})^2 \rangle = \frac{1}{45}k_c^4 + O(k_c^6). \end{aligned} \quad (\text{B60})$$

B.3. The drift-diffusion equation

We can now derive Equation (13) by generalizing the approach of Ref. [35]. First, we denote the probabilities of the particle being in states $Z_S(E)$ and $Z_B(E)$ by $P_1(E, t)$ and $P_2(E, t)$, respectively. We express the rate of change of $P_1(E, t)$ and $P_2(E, t)$ as

$$\begin{aligned} \frac{\partial P_1(E, t)}{\partial t} &= J_1^+(E, t) - J_1^-(E, t) \\ \frac{\partial P_2(E, t)}{\partial t} &= J_2^+(E, t) - J_2^-(E, t), \end{aligned} \quad (\text{B61})$$

where $J_{1,2}^+$ and $J_{1,2}^-$ are the in- and out-fluxes, respectively. Since the state of the particle has to alternate between Z_S and Z_B between steps of the energy-space random walk, we have

$$\begin{aligned} J_1^+(E, t) &= \int G_2(E|E') J_2^-(E', t) dE', \\ J_2^+(E, t) &= \int G_1(E|E') J_1^-(E', t) dE', \end{aligned} \quad (\text{B62})$$

where $G_{1,2}(E|E')$ are the energy transition probabilities for **D** and **S**, respectively. The out-fluxes $J_{1,2}^-$ can be written as

$$\begin{aligned} J_1^-(E, t) &= \phi_1(E, t) P_1(E, 0) + \int_0^t \phi_1(E, t-t') J_1^+(E, t') dt', \\ J_2^-(E, t) &= \phi_2(E, t) P_2(E, 0) + \int_0^t \phi_2(E, t-t') J_2^+(E, t') dt', \end{aligned} \quad (\text{B63})$$

where $\phi_{1,2}(E, t) = \phi_{D,S}(E, t)$ are the waiting-time distributions. The first terms in Equation (B63) represent the fluxes contributed by particles originally in the states 1, 2 at $t = 0$, and the second terms represent the fluxes contributed by particles that enter the states at t' and leave at t . Using Equation (B61), we eliminate $J_{1,2}^+$ from Equation (B63) and get

$$\begin{aligned} J_1^-(E, t) &= \phi_1(E, t) P_1(E, 0) + \int_0^t \phi_1(E, t-t') \frac{\partial P_1(E, t')}{\partial t'} dt' + \int_0^t \phi_1(E, t-t') J_1^-(E, t') dt', \\ J_2^-(E, t) &= \phi_2(E, t) P_2(E, 0) + \int_0^t \phi_2(E, t-t') \frac{\partial P_2(E, t')}{\partial t'} dt' + \int_0^t \phi_2(E, t-t') J_2^-(E, t') dt'. \end{aligned} \quad (\text{B64})$$

These integral equations can be solved using the Laplace transform, which gives

$$\begin{aligned} \tilde{J}_1^-(E, u) &= u \tilde{M}_1(E, u) \tilde{P}_1(E, u), \\ \tilde{J}_2^-(E, u) &= u \tilde{M}_2(E, u) \tilde{P}_2(E, u), \end{aligned} \quad (\text{B65})$$

with the memory kernels given by

$$\tilde{M}_{1,2}(E, u) = \frac{\tilde{\phi}_{1,2}(E, u)}{1 - \tilde{\phi}_{1,2}(E, u)}. \quad (\text{B66})$$

After Laplace-transforming back, Equation (B65) gives

$$\begin{aligned} J_1^-(E, t) &= \frac{d}{dt} \int_0^t M_1(E, t-t') P_1(E, t') dt', \\ J_2^-(E, t) &= \frac{d}{dt} \int_0^t M_2(E, t-t') P_2(E, t') dt'. \end{aligned} \quad (\text{B67})$$

Substituting this into Equation (B61) and using Equation (B62) to eliminate $J_{1,2}^+$, we get

$$\begin{aligned} \frac{\partial P_1(E, t)}{\partial t} &= \int \left[G_2(E|E') \frac{d}{dt} \int_0^t M_2(E', t-t') P_2(E', t') dt' \right] dE' - \frac{d}{dt} \int_0^t M_1(E, t-t') P_1(E, t') dt', \\ \frac{\partial P_2(E, t)}{\partial t} &= \int \left[G_1(E|E') \frac{d}{dt} \int_0^t M_1(E', t-t') P_1(E', t') dt' \right] dE' - \frac{d}{dt} \int_0^t M_2(E, t-t') P_2(E, t') dt'. \end{aligned} \quad (\text{B68})$$

Note that $G_{1,2}(E|E')$ is local, so we can perform a Kramer–Moyal expansion [34] to convert the above equation to a differential equation in E , and the results are

$$\begin{aligned} \frac{\partial P_1(E, t)}{\partial t} &= \frac{d}{dt} \int_0^t \left\{ -\frac{\partial}{\partial E} \left[D_2^{(1)}(E) M_2(E, t-t') P_2(E, t') \right] + \frac{1}{2} \frac{\partial^2}{\partial E^2} \left[D_2^{(2)}(E) M_2(E, t-t') P_2(E, t') \right] \right\} dt' \\ &\quad + \frac{d}{dt} \int_0^t \left[M_2(E, t-t') P_2(E, t') - M_1(E, t-t') P_1(E, t') \right] dt', \\ \frac{\partial P_2(E, t)}{\partial t} &= \frac{d}{dt} \int_0^t \left\{ -\frac{\partial}{\partial E} \left[D_1^{(1)}(E) M_1(E, t-t') P_1(E, t') \right] + \frac{1}{2} \frac{\partial^2}{\partial E^2} \left[D_1^{(2)}(E) M_1(E, t-t') P_1(E, t') \right] \right\} dt' \\ &\quad + \frac{d}{dt} \int_0^t \left[M_1(E, t-t') P_1(E, t') - M_2(E, t-t') P_2(E, t') \right] dt', \end{aligned} \quad (\text{B69})$$

where $D_{1,2}^{(n)}(E) = \int \Delta E^n G_{1,2}(E + \Delta E|E) d\Delta E$ are the Kramer–Moyal coefficients. In the current context, $D_{1,2}^{(1)}(E)$ correspond to $\mu_{S,D}(E)$, and $D_{1,2}^{(2)}(E)$ correspond to $\sigma_{S,D}^2(E)$. Since $\phi_{1,2}(E, t)$ is approximately exponential, we also have

$$M_{1,2}(E, t) \simeq \frac{1}{\tau_{1,2}(E)}, \quad (\text{B70})$$

where $\tau_{1,2}(E)$ are the mean waiting times $\langle T_{S,D} \rangle$ at energy E . Putting this in, we get the following set of Fokker–Planck equations:

$$\begin{aligned} \frac{\partial P_1(E, t)}{\partial t} &= \frac{P_2(E, t)}{\tau_2(E)} - \frac{P_1(E, t)}{\tau_1(E)} - \frac{\partial}{\partial E} \left[\frac{D_2^{(1)}(E)}{\tau_2(E)} P_2(E, t) \right] + \frac{1}{2} \frac{\partial^2}{\partial E^2} \left[\frac{D_2^{(2)}(E)}{\tau_2(E)} P_2(E, t) \right], \\ \frac{\partial P_2(E, t)}{\partial t} &= \frac{P_1(E, t)}{\tau_1(E)} - \frac{P_2(E, t)}{\tau_2(E)} - \frac{\partial}{\partial E} \left[\frac{D_1^{(1)}(E)}{\tau_1(E)} P_1(E, t) \right] + \frac{1}{2} \frac{\partial^2}{\partial E^2} \left[\frac{D_1^{(2)}(E)}{\tau_1(E)} P_1(E, t) \right]. \end{aligned} \quad (\text{B71})$$

With rapid relaxation [34], we have $P_2(E, t)/\tau_2(E) - P_1(E, t)/\tau_1(E) \simeq 0$ and

$$P_{1,2}(E, t) = \frac{\tau_{1,2}(E)}{\tau_1(E) + \tau_2(E)} P(E, t), \quad (\text{B72})$$

with $P(E, t) = P_1(E, t) + P_2(E, t)$. Substituting this into Equation (B71), we get

$$\frac{\partial P(E, t)}{\partial t} = -\frac{\partial}{\partial E} \left[\frac{D_1^{(1)}(E) + D_2^{(1)}(E)}{\tau_1(E) + \tau_2(E)} P(E, t) \right] + \frac{1}{2} \frac{\partial^2}{\partial E^2} \left[\frac{D_1^{(2)}(E) + D_2^{(2)}(E)}{\tau_1(E) + \tau_2(E)} P(E, t) \right]. \quad (\text{B73})$$

We finally get

$$\frac{\partial P(E, t)}{\partial t} = \frac{sfk_c^5}{45} \frac{\partial}{\partial E} \left[\frac{\partial}{\partial E} \left(\frac{1}{sk+f} P \right) - \frac{f}{2(sk+f)^2 E} P \right], \quad (\text{B74})$$

or, after some manipulation,

$$\frac{\partial P(E, t)}{\partial t} = \frac{sfk_c^5}{45} \frac{\partial}{\partial E} \left[\frac{1}{sk+f} \left(\frac{\partial P}{\partial E} - \frac{P}{2E} \right) \right], \quad (\text{B75})$$

which is Equation (13).

Appendix C. Non-equilibrium fluctuation–dissipation relation

In cases where the dynamics of a periodically driven and thermally isolated system obeys an energy-space drift-diffusion equation of the form

$$\frac{\partial P}{\partial t} = -\frac{\partial}{\partial E}[A(E)P] + \frac{1}{2}\frac{\partial^2}{\partial E^2}[B(E)P], \quad (\text{C76})$$

Ref. [29] proposed a general relation between the system-dependent drift and diffusion coefficients ($A(E)$ and $B(E)$, respectively),

$$2A(E) = \beta_T(E)B(E) + \frac{\partial}{\partial E}B(E), \quad (\text{C77})$$

where $\beta_T(E) = \partial_E \ln \Omega(E)$ is the micro-canonical inverse temperature defined via the density of states $\Omega(E)$. This relation is the non-equilibrium version of the equilibrium fluctuation–dissipation theorems, but its range of validity is not well established.

In our case, $\Omega(E) \sim \sqrt{E}$ and $\beta_T = 1/(2E)$. Reading off $A(E)$ and $B(E)$ from Equation (B74) shows that Equation (C77) is satisfied by our drift-diffusion equation in all regimes. This is not surprising because our drift-diffusion equation is derived from a semi-classical kinetic equation (Equation (4)) with reciprocal transition probabilities, $\mathcal{T}(\mathbf{k} \rightarrow \mathbf{k}') = \mathcal{T}(\mathbf{k}' \rightarrow \mathbf{k})$. This reciprocity implies that a system with equal occupation in every state [a uniform $n_k(\mathbf{k})$] must be a stationary state. Correspondingly, when $P(E) \sim \Omega(E)$, the probability current $J(E) = A(E)P(E) - (1/2)\partial_E[B(E)P(E)]$ should be zero, and this implies Equation (C77) as discussed in Ref. [29].

References

- [1] G. Martirosyan, C. J. Ho, J. Etrych, Y. Zhang, A. Cao, Z. Hadzibabic, C. Eigen, “Observation of subdiffusive dynamic scaling in a driven and disordered Bose gas”, 2023, preprint, <https://arxiv.org/abs/2304.06697>.
- [2] M. Kardar, *Statistical Physics of Fields*, Cambridge University Press, Cambridge, 2007.
- [3] T. Nakayama, K. Yakubo, R. L. Orbach, “Dynamical properties of fractal networks: Scaling, numerical simulations, and physical realizations”, *Rev. Mod. Phys.* **66** (1994), p. 381-443.
- [4] T. Halpin-Healy, Y.-C. Zhang, “Kinetic roughening phenomena, stochastic growth, directed polymers and all that. Aspects of multidisciplinary statistical mechanics”, *Phys. Rep.* **254** (1995), p. 215-414.
- [5] G. Ódor, “Universality classes in nonequilibrium lattice systems”, *Rev. Mod. Phys.* **76** (2004), p. 663-724.
- [6] A. Polkovnikov, K. Sengupta, A. Silva, M. Vengalattore, “Colloquium: Nonequilibrium dynamics of closed interacting quantum systems”, *Rev. Mod. Phys.* **83** (2011), p. 863-883.
- [7] U. C. Täuber, *Critical Dynamics: A Field Theory Approach to Equilibrium and Non-Equilibrium Scaling Behavior*, Cambridge University Press, Cambridge, 2014.
- [8] E. Altman, R. Vosk, “Universal dynamics and renormalization in many-body-localized systems”, *Annu. Rev. Condens. Matter Phys.* **6** (2015), no. 1, p. 383-409.
- [9] T. Langen, R. Geiger, J. Schmiedmayer, “Ultracold atoms out of equilibrium”, *Annu. Rev. Condens. Matter Phys.* **6** (2015), no. 1, p. 201-217.
- [10] M. A. Muñoz, “Colloquium: Criticality and dynamical scaling in living systems”, *Rev. Mod. Phys.* **90** (2018), article no. 031001.
- [11] A. N. Mikheev, I. Siovitz, T. Gasenzer, “Universal dynamics and non-thermal fixed points in quantum fluids far from equilibrium”, 2023, preprint, <https://arxiv.org/abs/2304.12464>.
- [12] Y. Sagi, M. Brook, I. Almog, N. Davidson, “Observation of anomalous diffusion and fractional self-similarity in one dimension”, *Phys. Rev. Lett.* **108** (2012), article no. 093002.
- [13] C.-L. Hung, V. Gurarie, C. Chin, “From cosmology to cold atoms: Observation of Sakharov oscillations in a quenched atomic superfluid”, *Science* **341** (2013), no. 6151, p. 1213-1215.
- [14] P. Makotyn, C. E. Klauss, D. L. Goldberger, E. A. Cornell, D. S. Jin, “Universal dynamics of a degenerate unitary Bose gas”, *Nat. Phys.* **10** (2014), p. 116-119.
- [15] N. Navon, A. L. Gaunt, R. P. Smith, Z. Hadzibabic, “Emergence of a turbulent cascade in a quantum gas”, *Nature* **539** (2016), p. 72-75.

- [16] M. Prüfer, P. Kunkel, H. Strobel, S. Lannig, D. Linnemann, C.-M. Schmied, J. Berges, T. Gasenzer, M. K. Oberthaler, “Observation of universal dynamics in a spinor Bose gas far from equilibrium”, *Nature* **563** (2018), no. 7730, p. 217-220.
- [17] C. Eigen, J. A. P. Glidden, R. Lopes, E. A. Cornell, R. P. Smith, Z. Hadzibabic, “Universal prethermal dynamics of Bose gases quenched to unitarity”, *Nature* **563** (2018), no. 7730, p. 221-224.
- [18] S. Erne, R. Bücker, T. Gasenzer, J. Berges, J. Schmiedmayer, “Universal dynamics in an isolated one-dimensional Bose gas far from equilibrium”, *Nature* **563** (2018), no. 7730, p. 225-229.
- [19] S. P. Johnstone, A. J. Groszek, P. T. Starkey, C. J. Billington, T. P. Simula, K. Helmerson, “Evolution of large-scale flow from turbulence in a two-dimensional superfluid”, *Science* **364** (2019), no. 6447, p. 1267-1271.
- [20] R. Saint-Jalm, P. C. M. Castilho, E. Le Cerf, B. Bakkali-Hassani, J.-L. Ville, S. Nascimbene, J. Beugnon, J. Dalibard, “Dynamical symmetry and breathers in a two-dimensional Bose gas”, *Phys. Rev. X* **9** (2019), article no. 021035.
- [21] J. A. P. Glidden, C. Eigen, L. H. Dogra, T. A. Hilker, R. P. Smith, Z. Hadzibabic, “Bidirectional dynamic scaling in an isolated Bose gas far from equilibrium”, *Nat. Phys.* **17** (2021), no. 4, p. 457-461.
- [22] M. Gałka, P. Christodoulou, M. Gazo, A. Karailiev, N. Dogra, J. Schmitt, Z. Hadzibabic, “Emergence of isotropy and dynamic scaling in 2D wave turbulence in a homogeneous Bose gas”, *Phys. Rev. Lett.* **129** (2022), article no. 190402.
- [23] D. Wei, A. Rubio-Abadal, B. Ye, F. Machado, J. Kemp, K. Srakaew, S. Hollerith, J. Rui, S. Gopalakrishnan, N. Y. Yao, I. Bloch, J. Zeiher, “Quantum gas microscopy of Kardar–Parisi–Zhang superdiffusion”, *Science* **376** (2022), no. 6594, p. 716-720.
- [24] Y. Le, Y. Zhang, S. Gopalakrishnan, M. Rigol, D. S. Weiss, “Observation of hydrodynamization and local prethermalization in 1D Bose gases”, *Nature* **618** (2023), p. 494-499.
- [25] S. Huh, K. Mukherjee, K. Kwon, J. Seo, S. I. Mistakidis, H. R. Sadeghpour, J.-Y. Choi, “Classifying the universal coarsening dynamics of a quenched ferromagnetic condensate”, 2023, preprint, <https://arxiv.org/abs/2303.05230>.
- [26] N. Navon, C. Eigen, J. Zhang, R. Lopes, A. L. Gaunt, K. Fujimoto, M. Tsubota, R. P. Smith, Z. Hadzibabic, “Synthetic dissipation and cascade fluxes in a turbulent quantum gas”, *Science* **366** (2019), no. 6463, p. 382-385.
- [27] C. Jarzynski, W. J. Swiatecki, “A universal asymptotic velocity distribution for independent particles in a time-dependent irregular container”, *Nucl. Phys. A* **552** (1993), no. 1, p. 1-9.
- [28] C. Jarzynski, “Energy diffusion in a chaotic adiabatic billiard gas”, *Phys. Rev. E* **48** (1993), p. 4340-4350.
- [29] G. Bunin, L. D’Alessio, Y. Kafri, A. Polkovnikov, “Universal energy fluctuations in thermally isolated driven systems”, *Nat. Phys.* **7** (2011), no. 11, p. 913-917.
- [30] W. Hodson, C. Jarzynski, “Energy diffusion and absorption in chaotic systems with rapid periodic driving”, *Phys. Rev. Res.* **3** (2021), article no. 013219.
- [31] W. Hodson, C. Jarzynski, “Energy diffusion and prethermalization in chaotic billiards under rapid periodic driving”, *Phys. Rev. E* **104** (2021), article no. 064210.
- [32] L. E. Reichl, W. A. Lin, “Exact quantum model of field-induced resonance overlap”, *Phys. Rev. A* **33** (1986), p. 3598-3601.
- [33] W. A. Lin, L. E. Reichl, “Spectral analysis of quantum-resonance zones, quantum Kolmogorov-Arnold-Moser theorem, and quantum-resonance overlap”, *Phys. Rev. A* **37** (1988), p. 3972-3985.
- [34] C. Gardiner, *Handbook of Stochastic Methods*, Springer, Heidelberg, 1985.
- [35] J. Klafter, I. M. Sokolov, *First Steps in Random Walks: From Tools to Applications*, Oxford University Press, Oxford, 2011.
- [36] K. S. Fa, E. K. Lenzi, “Power law diffusion coefficient and anomalous diffusion: Analysis of solutions and first passage time”, *Phys. Rev. E* **67** (2003), article no. 061105.
- [37] E. Abrahams (ed.), *50 Years of Anderson Localization*, World Scientific, Singapore, 2010.